Permeation of particle through a four-helix-bundle model channel

Bin Xue, Yu Su, and Wei Wang[a)]
National Solid State Microstructure Laboratory, Institute of Biophysics and Department of Physics, Nanjing University, Nanjing 210093, People's Republic of China

(Received 11 June 2004; accepted 9 December 2004; published online 7 March 2005)

By using molecular dynamics simulation, the dynamic behaviors of particle permeation through a four-helix-bundle model channel are studied. The interior cavity of the four-helix-bundle provides the "routes" for particle permeation. The main structural properties of the model channel are similar to those that appear in natural four-helix-bundle proteins. It is found that the interior structure of the model channel may greatly influence the permeation process. At the narrow necks of the model channel, the particle would be trapped during the permeation. There is a threshold value for the driving force. When the driving force is larger than this threshold value, the mean first permeation time decreases sharply and tends to be saturated. Increasing the temperature of either the model channel or the particle reservoir can also facilitate the permeation. Enhancing the interaction strength between the particle and monomer on the four-helix-bundle model chain will hinder the permeation. Hence, the electrical current which is induced by the particle permeation is a function of the driving force and temperature. It is found that this current increases monotonically as the strength of the driving force or the temperature increases, but decreases as the interaction strength between the particle and monomer increases. It is also found that the larger the friction coefficient, the slower the permeation is. In addition, the multiparticle (or multi-ion) permeation process is also studied. The permeation of multiparticle is usually quicker than that of the single particle. The permeation of particle through a five-helix-bundle shows similar properties as that through a four-helix-bundle. © *2005 American Institute of Physics*. [DOI: 10.1063/1.1854620]

I. INTRODUCTION

Ion channel is one kind of important transmembrane protein. It keeps the concentration balance of various ions between extracellular and intracellular environments and transduces signals into or out of the cell. Disabling the function of the ion channel may lead to many diseases in human body. The study on ion channels has achieved a lot of progress both experimentally and theoretically since the crystal structure of potassium channel KcsA was solved and found to be composed of four helical domains.[1] The common conformational features of most ion channel proteins are[2] (1) every channel is composed of several similar subunits; (2) the channel can be divided into three parts according to their relevant positions in the cellular membrane, which are the extracellular part, the cytoplasmic (intracellular) part, and the central transbilayer part. In the case of a rough approximation for potassium channel, the extracellular part of the channel plays an important role in the ion selectivity, while the cytoplasmic part seems to be responsible for gating. The transmembrane part of the ion channel has a cavity surrounded by the subunits of the ion channel protein and facilitates ions to permeate through the lipid bilayer.

The conformation and the number of the subunits composing the channel cavity are different for various kinds of channels. The potassium channel KcsA has four subunits which are composed of a number of helices and loops.[1,3] The M2 proton channel in influenza A virus is also a tetrameric α-helix bundle.[4] The high-voltage gated calcium channel is a multi-subunit complex.[5] The mechanosensitive channel MscL takes the form of homopentamer.[6] The ligand-gated channel nicotinic acetylcholine receptor nAChR has an assembly of five α-helix bundle.[7] Porin is a trimeric β barrel protein.[8,9] Hemolysin is a heptameric β-strand barrel.[10] Besides, many artificial ion channels, which are important for engineering applications and theoretical studies,[11–14] have similar structural properties as the natural ion channels have.

Previous experiments have revealed that almost all ion channels have the ability to select specific kinds of ions and allow them to pass through. This is the characteristic of the channel selectivity. Besides the selectivity, the channel itself can change its conformation to facilitate the running of specific ions. This relates to the process of gating.[15] To understand the functions and working mechanisms of various ion channels, many models have been proposed. These models try to explain the relation between structure and function of ion channels, and to depict the behaviors of ions in the channel. Among various models, the all-atomic molecular dynamics (MD) model is well known, and has been applied to investigate: (1) the energetics of ion conduction through the potassium channel;[16] (2) the structural properties of M2 channel protein;[17] (3) the potassium and sodium selectivity of potassium channel;[18] (4) the structural and dynamic properties of a synthetic four-helix model channel.[19] It has also been used to test the appropriateness of the force fields in the study of channels.[20] Recently, a model combining the all-atomic consideration and an irregular chamber has been

[a)]Author to whom correspondence should be addressed. Electronic mail: wangwei@nju.edu.cn

adopted to explain the selectivity of potassium channel[21] and the ligand-gated channels.[7] Besides, a lumen model with idealized internal surface is also used to investigate the selectivity and permeation of potassium channel[22] and calcium channel.[23] The chamber model treats the subunits around the cavity as a wall which loses almost all the structural information of the cavity.[21,23]

However, it is well known that the all atomic MD simulation is quite time consuming and is limited to only several nanoseconds which is far shorter than the normal permeation time of ions (tens of nanoseconds).[18] Is it possible to make a coarse-grained model for ion channel without losing too much local structural information of the subunits of the channel protein and, in the meantime, with reachable simulation time range of the permeation process for particle?

Here in this paper, a study on the permeation of particle passing through a coarse-grained model of ion channel is reported. In this model, the ion channel is simplified as a bundle of four helices with each bead acting as one amino acid residue, and the structural properties of the protein have been preserved. Thus, the simulation at the all-atom level which is very time consuming can be avoided. The emphasis of this model is neither on the ion selectivity nor on the gating but on the permeation process which is the running of ion through the cavity of the model channel. The reasons are threefold. First, the permeation process and the impact of the local structures of the channel on the ion's mobility are important. For example, the permeation of particles in channel-like proteins, such as the hemolysins and porins, is of specific interest since the selectivity is not so important as that in the selective ion channels. Second, the permeation of particles is one of the main functions in the artificial ion channels and is dominated by the interior structures which are designed distinctively for different artificial channels.[11,24] Third, the moving of particles along a complicated force field is also an interesting topic.

Thus, the detailed dynamic behaviors of particle permeation through a four-helix-bundle model channel are simulated by molecular dynamics. It is found that the interior structure of the model channel can greatly influence the permeation process. When the driving force is larger than a threshold value, the mean first permeation time (MFPT) decreases sharply and tends to be saturated. The electrical current which is induced by the permeation of electrically charged particle, increases monotonically as the strength of the driving force or the temperature increases, but decreases as the interaction strength between the particle and monomer increases. The multiparticle (or multi-ion) permeation process is also studied. It is found that the permeation of multiparticle is usually quicker than that of the single particle.

This paper is arranged as follows. In Sec. II, the model of channel and the methods for simulations are introduced. In Sec. III, the results and discussions are presented. In the final section, a summary is given.

II. METHOD

A. Channel model

The model of ion channel used in this paper follows a simplified protein model introduced by Thirumalai and co-workers.[25] They simulate the folding behavior of a four-helix-bundle model protein which is artificially synthesized by Degrado and collaborators.[26] The same kind of artificially synthesized protein also shows the property of single-channel current,[24] indicating that this model protein is similar to the natural ion channel. In Thirmualai's work, the four-helix-bundle protein is modeled by a heteropolymer chain of 73 monomers or beads. The chain has four identical helical sequences separated by three same loop sequences. Each helical sequence has six hydrophobic (B) and ten hydrophilic (P) monomers. The alignment of monomers in one helical sequence is

$$(H) = -PPBPPBBPPBPPBBPP-.$$

The loop sequence is composed of three neutral (N) monomers and can be represented by

$$(L) = -NNN-.$$

Thus, the alignment of the 73-monomer-heteropolymer is

$$(\text{Chain}) = H-L-H-L-H-L-H.$$

The arrangement of such a sequence makes the heteropolymer chain have a native conformation of the four-helix-bundle. Each monomer in the chain is treated as a bead with a certain radius. This radius provides the effect of excluded volume.

B. Potential energy

The total potential energy of the heteropolymer chain is a summation of the bond interactions between consecutive beads (U_{bond}), the bond angle interactions ($U_{\text{bond-angle}}$), the dihedral angle interactions (U_{dihedral}), and the long-range Lennard-Jones interactions (U_{LJ}) among beads separated by at least three bonds,

$$U = U_{\text{bond}} + U_{\text{bond-angle}} + U_{\text{dihedral}} + U_{\text{LJ}}. \tag{1}$$

The interaction between every two consecutive beads represents the covalent bonds in the heteropolymer chain, and is modeled by a quadratic and quartic potential,[27]

$$U_{\text{bond}} = \sum_{j=1}^{N-1} k_1(r_{j,j+1} - d_0)^2 + k_2(r_{j,j+1} - d_0)^4, \tag{2}$$

where $r_{j,j+1}$ is the distance between two consecutive beads j and $j+1$ in the simulation, d_0 is the equilibrium length of the bond and is set to be 3.8 Å. The value of 3.8 Å corresponds to the length of a *trans* peptide bond.[28] $k_1 = \varepsilon$ and $k_2 = 100\varepsilon$ are the interaction strengths with ε being the unit of reduced energy. The quadratic term characterizes the consecutive beads as a harmonic oscillator, while the quartic term acts as a "soft clamp" whose function is to restrict the beads within a distance not far away from the equilibrium position d_0.

The bond angle interaction is also defined by a harmonic potential,

$$U_{\text{bond-angle}} = \sum_{j=1}^{N-2} \frac{1}{2} k_\theta (\theta_j - \theta_0)^2, \tag{3}$$

in which $k_\theta = 20\varepsilon/(\text{rad})^2$ is the bond angle interaction strength. θ_j is the value of the jth bond angle, $\theta_0 = 105°$ is its equilibrium value.

There are two types of dihedral angle potentials which depends on the characteristics of the monomers involved in forming the dihedral angle.[25] In the helical regions where the monomers are either hydrophobic (B) or hydrophilic (P), the dihedral angle potential is represented by

$$U^H_{\text{dihedral}} = \sum_j [A_\phi(1 - \cos\phi_j) + B_\phi(1 + \cos\phi_j) + C_\phi(1 + \cos(\phi_j + \pi/4)]. \tag{4}$$

Here the summation is over all the dihedral angles in the helical regions. ϕ_j is the jth dihedral angle in these helical regions. $A_\phi = B_\phi = C_\phi = 1.6$ are the interaction strengths of the dihedral angle. Whereas in the loop regions where the neutral monomer (N) is involved, the dihedral angle potential is

$$U^L_{\text{dihedral}} = \sum_j D_\phi(1 + \cos 3\phi_j), \tag{5}$$

where ϕ_j is the jth dihedral angle in the loop regions. $D_\phi = 0.2$ is chosen to reflect the flexibility of loop region.

For the interaction between two beads separated by at least three bonds, there are also two types of Lennard-Jones interactions.[25] The interaction between two hydrophobic monomers is attractive at large spatial distance, hence a 12-6 Leonard–Jones (LJ) potential is used as

$$U^B_{\text{LJ}} = \sum_{i,j} 4\lambda\varepsilon \left[\left(\frac{\sigma_{ij}}{r_{ij}} \right)^{12} - \left(\frac{\sigma_{ij}}{r_{ij}} \right)^{6} \right]. \tag{6}$$

Here λ is a scaling factor for the interaction and its value is chosen as $\lambda = 1.7$. r_{ij} is the distance between two nonconsecutive beads i and j, σ_{ij} is the equilibrium distance between them, and here we set the values of σ_{ij} to be the eqilibrium distance between two consecutive monomers. The interaction between one nonhydrophoboic monomer (i.e., L or N) and another monomer of any other type is assumed to be purely repulsive. Thus we have

$$U^P_{\text{LJ}} = \sum_{i,j} 4\lambda\varepsilon \left(\frac{\sigma_{ij}}{r_{ij}} \right)^{12}. \tag{7}$$

Here λ, σ_{ij}, and r_{ij} are the same quantities as mentioned above.

The moving ion is simplified as a neutral particle in most cases during the simulation of the permeation. This simplification is reasonable in the coarse-grained model since almost all the residues in the transbilayer part are electrically neutral in KcsA and many other ion channels. The synthetic channels peptide used by Lear (1988) is also composed of electrically neutral animo acids, namely, Leucine and Serine. The interaction between a particle and a monomer is set to be

$$U_{IM} = \sum_j 4\lambda\varepsilon_{IM} \left[\left(\frac{\sigma_{IM}}{r_{I,j}} \right)^{12} - \left(\frac{\sigma_{IM}}{r_{I,j}} \right)^{6} \right]. \tag{8}$$

Here the summation is over all the monomers in the heteropolymer chain. $r_{I,j}$ is the distance between the jth monomer and the ion (particle). $\lambda = 1.7$ is the scaling factor for the interaction, and $\sigma_{IM} = 2.0$ Å is adopted. The reasons are that the radius of the narrowest part of the four-helix-bundle is around 2 Å, and the van der Waals (Vdw) radii of hydrogen, oxygen, and potassium are around 1 Å or slightly larger.

In the case of multiparticle, a repulsive potential is applied to model the repulsion between two ions of identical electricity

$$U_{II} = \sum_{jj \neq i} 4\lambda_{II}\varepsilon \left(\frac{\sigma_{II}}{r_{ij}} \right)^2. \tag{9}$$

This gives the interaction on the ith particle by all other particles. $\lambda_{II} = 1.7$ is another scaling factor for the interaction between particles. σ_{II} is taken as $\sigma_{II} = 2.0$ Å, τ_{ij} is the distance between the ith and jth particle. The potential is a relative long-range interaction between particles.

C. Langevin dynamics

Langevin dynamics[29] is applied to proceed with the evolution of the channel system and the permeation of particles

$$\frac{d^2\mathbf{r}_\text{i}}{dt^2} = -\xi\frac{d\mathbf{r}_\text{i}}{dt} + (\mathbf{F}_\text{i} + \mathbf{\Gamma}_\text{i} + \mathbf{F}_\text{d})/\mathbf{m}_\text{i}. \tag{10}$$

Here reduced units are adopted based on $\tau = a\sqrt{m/\varepsilon}$, in which τ is the characteristic time of the system, a is the bond length d_0 and m is the mass of each monomer.[30] m_i is the mass of the ith monomer or the particle depending on which one in the particle and the monomer is described in this formula. $\mathbf{r}_\text{i}$ is the position vector of the ith monomer or particle, ξ is the friction coefficient and varies from 0.05 to 10.0 in the simulations. The maximal friction coefficient used above is about one order less than the friction of N_a^+ in bulk water. $\mathbf{F}_\text{i} = -\nabla\mathbf{U}$ is the conformational force, U is total potential of the monomer or the particle. $\mathbf{F}_d$ is the driving force acting on the particle which originates from the electrical force caused by the membrane voltage. The electrical driving force can be simplified as $\mathbf{F}_d = \Delta U q/\Delta d$, where ΔU is the membrane voltage, q is the quantity of electrical charges on one particle, and Δd is the thickness of the membrane. In the reduced units, the unit of force is ε/d_0. If we take $\Delta U = 60$ mV, $q = 1.6 \times 10^{-19}$ C, and $\Delta d = 40$ Å, we have $\mathbf{F}_d \sim 0.2\varepsilon/d_0$. The term of driving force is only eligible for the particle. $\mathbf{\Gamma}_\text{i}$ is the random force satisfying

$$\langle \mathbf{\Gamma}_i(t) \rangle = 0, \quad \langle \mathbf{\Gamma}_i(t)\mathbf{\Gamma}_j(t') \rangle = 6k_B T\xi\delta_{ij}\delta(t - t'). \tag{11}$$

The subscript indicates the index of the monomer or the particle. k_B is the Boltzmann constant. T is the reduced temperature. The friction coefficient satisfies Stocks' law $\xi = 6\pi\eta a/m$, where η is the viscosity of the solvant, a and m are the radius and the mass of the monomer or the particle, respectively. If the monomer is assumed to have a volume of 140 Å^3 and a weight of 100 Da, then the monomer has roughly the same friction coefficient as the potassium ion

has. Note that the difference in Eq. (10) for the particle or the monomer is only in the presence or the absence of the term of driving force.

Leap-frog algorithm is applied to solve the Langevin's equation, Eq. (10),[29]

$$\dot{\mathbf{r}}_i\left(t+\tfrac{1}{2}h\right) = (1-\alpha\xi)\dot{\mathbf{r}}_i\left(t-\tfrac{1}{2}h\right) + \alpha[\mathbf{\Gamma}_i(t) + \mathbf{F}_i(t) + \mathbf{F}_d(t)],$$

$$\mathbf{r}_i(t+h) = \mathbf{r}_i(t) + h\dot{\mathbf{r}}_i\left(t+\tfrac{1}{2}h\right). \tag{12}$$

Here $\alpha=(h/m)/[1+(h/2m)\xi]$, h is the integration time step and is set to be $h=0.0005\tau$ due to the small mass of the ion, which corresponds to a real time of 1.5 fs.

In order to obtain the native conformation of the heteropolymer chain, simulated annealing is used. The initial conformation of the heteropolymer chain is open, and the initial velocities follow the Maxwell's distribution at the given temperature T.

D. Analyzed quantities

To show the detailed structural information of the four-helix-bundle, the cross angles between adjacent helical subunits are calculated. First the direction vector of each subunit is obtained by

$$\mathbf{R}_s = \frac{1}{2M}\sum(\mathbf{r}_{i+3} + \mathbf{r}_{i+4} - 2\mathbf{r}_i). \tag{13}$$

Here $\mathbf{R}_s$, is the vector of each helical subunit which is an average of the vectors among 1–4 pairs and 1–5 pairs of monomers. M is the maximal number of 1–4 pairs in one subunit. Since each subunit has 16 monomers, one has $M=12$. $\mathbf{r}_{i+3}$, and $\mathbf{r}_{i+4}$, and $\mathbf{r}_i$ are position vectors for the $(i+3)$th, $(i+4)$th, and ith monomers, respectively. For the accuracy of statistics, only 12 monomers in the middle part of each subunit are taken to calculate the subunit vector. In such a case, one has $M=8$. Then the cross angle between two subunits $\Omega_{i,i+1}$ can be obtained from

$$\cos\Omega_{i,i+1} = \cos\alpha_i\cos\alpha_{i+1} + \cos\beta_i\cos\beta_{i+1} + \cos\gamma_i\cos\gamma_{i+1}. \tag{14}$$

Here $\cos\alpha_i$, $\cos\beta_i$, $\cos\gamma_i$, and $\cos\alpha_{i+1}$, $\cos\beta_{i+1}$, $\cos\gamma_{i+1}$ are the direction cosines for the ith and the $(i+1)$th subunits, accordingly.

To measure the moving of the particle in the channel, the permeation time, which is the ensemble average of the total time steps for the particle to pass through the channel, is used. To obtain an ensemble average, up to 200 times of simulations with different initial conditions are proceeded. Then the average permeation time over all the runnings is defined as the MFPT, i.e., τ_M. The maximal simulation time is 2×10^7 steps which corresponds to a real time of 30 ns. When the particle fails to pass through the channel within the total simulation steps or diffuse into the lateral of the cavity, i.e., out of the channel, the permeation time is set to be 2×10^7. A variation rate of MFPT, Q_A, with respect to a specific interested physical quantity A is defined as

$$Q_A = \frac{\Delta\tau_M}{\Delta A}, \tag{15}$$

where ΔA is the variation of A, $\Delta\tau_M$ is the respective increment of MFPT when A is changed by ΔA.

The energy profile of particle is applied to show the change of potential energy along the channel axis. When calculating the energy profile, the particle is moved artificially along the channel axis (z axis). At each position of z, the particle is only allowed to move in the plane perpendicular to the z axis and equilibrate in this plane for 6×10^5 time steps. Then the average potential energy during this equilibration is plotted as a function of the z axis.[23]

To study the influence on the permeation of ion concentration, a particle reservoir is introduced just above the top of the channel. The particle reservoir is a cylinder box with radius of 8 Å and height of 20 Å, so the volume of the box is 4.02×10^3 Å^3. The concentration of particle is about 0.4 mol/L when one particle is in such a box. To simulate the permeation of particle(s) under various concentrations, different number of particles are placed randomly in the cylinder box. The simulation steps needed by a particle to enter the open mouth of the channel from the cylinder box is defined as the selection rate τ_S. The time of passing through the channel for a particle after entering the open mouth is considered as the permeation time mentioned above. The simulations show that the selection rate is usually one order of magnitude faster than the permeation time. Hence, as a reasonable approximation in this model, the selection could be regarded as a continuous process and only the permeation time of a particle is taken to describe the process of running through the model channel. Then the transmembrane electrical current can be obtained by $I=n_q q/(\tau_M+\tau_S)$. Here n_q is the valence of the particle, and q is the unit electrical charge.

To investigate the multiparticle permeation process, i.e., many particles passing through the channel simultaneously, the multiparticle energy profile[23] and the multiparticle trajectories[18] are used.

The multiparticle energy profile shows the energetic impact on one particle of other particles. In the case of two particles, the first particle is fixed at a specific position in the channel, and the second particle is moved along the helical bundle axis (Z axis) with a distance of 1 Å for each times. Then the second particle is equilibrated for 6×10^5 time steps at each position of Z. During the equilibrations, the second particle is restricted to move only in the plane perpendicular to the Z axis. The average energy of the second particle in the equilibration is taken as the potential energy corresponding to the specific Z axis. This average energy provides the potential information of the second particle under the influence of the first particle. Hence, the relation between the average energy and the position at Z axis of the second particle is called the multiparticle energy profile. When three particles are involved the first two particles are located at specific positions in the channel and the third particle is moved along the Z axis in the same way as mentioned above. Then the potential energy of the third particle as a function of Z axis is obtained by using the above defined protocols.

The dynamic energy profile is also applied to show the dynamic process of permeation. Suppose there are already two particles in the channel aligned in Z direction. The first particle is near to the intracellular and the second particle is close to the extracellular. Then the energy profile of the third particle may be different from the above described single particle energy profile. In this case, new potential wells may be created at positions near the extracelluar. When the third particle enters the channel from the extracellular, it can stay in these new potential wells or jump to nearby wells which are separated by low energy barriers. Hence, the third particle may move close to the second particle and have strong influence on the second particle's energy profile. Under this interaction, the second particle will be pushed to new possible wells near its previous position. And last, the first particle's energy profile will also be changed under the influence of the second particle. This is somewhat a dynamic process, hence the energy profile obtained in this way is named after "dynamic energy profile." Other simulation details in obtaining the dynamic energy profile are the same as in caculating the normal multiparticle energy profile.

The trajectories of all particles can be obtained to show the dynamic multiparticle permeation process. In the case of two particles, the first particle is located in the channel at a specific position in advance and the second particle is put near to the open mouth, then the simulation begins. The trajectories of both particles are recorded. When studying the permeation of three particles, the first two particles are set in the channel at certain positions, and the third particle is released at the extracellular to start the simulation. All the trajectories for three particles are then recorded for further analysis.

III. RESULTS AND DISCUSSION

A. Channel properties

The native conformation of the four-helix-bundle model channel is shown is Fig. 1(a) in the backbone presentation. The particle is put above the top of the four-helix-bundle. The two loops of the bundle form the open mouth and are considered as the extracellular part. The bottom part of the bundle, i.e., the "C" and "N" termini of the chain, is modeled as the intracellular part. The length of the bundle is about 35 Å which is set as the length of the model channel. This length is in accordance with the typical thickness of membrane.[3] The Z axis is along the axis of the helical bundle. It has been observed experimentally that the cross angles between adjacent helical subunits in many natural four-helix-bundle proteins are about 10°–20°.[31–33] In our four-helix-bundle model channel, the equilibrium values of cross angles between subunits are $\Omega_{1,2}=17°$, $\Omega_{2,3}=21°$, $\Omega_{3,4}=15°$, and $\Omega_{4,1}=22°$, respectively. The subscripts are the indices of the subunits. These angles are basically the same as the values of the natural proteins.

Figures 1(b) and 1(c) show more detailed information of the conformation of the bundle. Figure 1(b) is viewed from the top of the channel. Each small circle with a number in it indicates a monomer and its sequential index along the chain. It is clear that the monomers distribute almost symmetrically around the center of the bundle. The central thick dashed circle depicts the pore of the channel with a radius of about 2 Å which is more or less the same as the radius of the narrowest part in potassium channel KcsA.[3] The bold line runs along the first helical subunit, i.e., from the 1st monomer to the 16th monomer (the other three subunits are not connected and not shown with bold line). From this line, it is obvious that each subunit has both inner side and outer side.

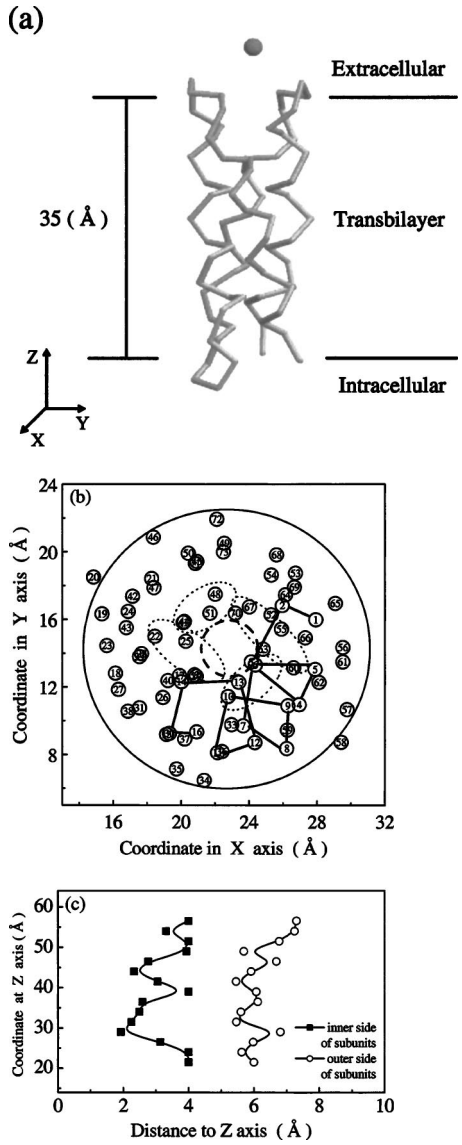

FIG. 1. The structural profile of the coarse-grained four-helix bundle model channel. (a) is the backbone picture of the four-helix bundle model channel; upside is the extracellular; underside is the intracellular; the particle above the bundle is the model of ion. Two loops at the upside form the open mouth. Both termini are in the intracellular. The full length of the model channel is around 35 Å. The equilibrium values of cross angles between subunits are $\Omega_{1,2}=17°$, $\Omega_{2,3}=21°$, $\Omega_{3,4}=15°$, and $\Omega_{4,1}=22°$, respectively. (b) The projection from upside to underside. Every circle with a number in it is a monomer forming the four-helix-bundle. The number is the index of that monomer. The central dashed circle depicts the inner pore of the model channel. The four dashed elliptic circles around the dashed circle are the inner sides of four subunits of the bundle. The outside dashed circle is the outer most boundary of the model channel. The bold line depicts the first subunit which is composed of monomers from the 1st to the 16th. (c) shows the statistical distance distribution of monomers away from Z axis. The filled squares on the left of the graph are for inner sides of four subunits. The open circles on the right of the figure are for the outer sides of four subunits.

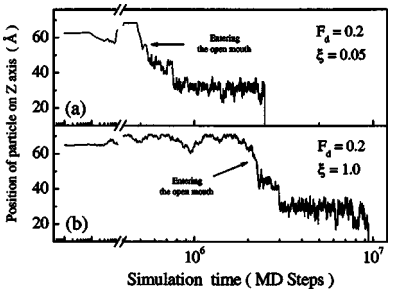

FIG. 2. Two typical permeation processes. The abscissa is on the base of logarithm. The driving force is $F_d=0.2$; the simulation temperature is $T=0.1$. The friction coefficients are (a) $\xi=0.05$ and (b) $\xi=1.0$, respectively.

The four dashed elliptic circles show four inner sides of four subunits, respectively. Apparently, all the subunits are not parallel to Z axis. The cross angles of subunits with respect to Z axis are $\Omega_{1,Z}=28°$, $\Omega_{2,Z}=4°$, $\Omega_{3,Z}=24°$, and $\Omega_{4,Z}=14°$, accordingly. The four inner sides compose a pore or a channel for the particle permeation. The perimeter along the four dashed elliptic circles is the boundary for inner sides. The largest solid circle shows the outer sides of the pore with radius about 7 Å.

Figure 1(c) is the distance distribution of monomers away from Z axis. The filled squares on the left of the graph are the average distances of the inner sides away from Z axis at each position of Z. The open circles on the right are the average distances of the outer sides of all subunits apart from Z axis. The distances to Z axis of monomers on inner parts of subunits vary from 2 to 4 Å. At around $Z\sim30$ Å, the radius of the pore reaches the overall minimum of $R_P\sim2$ Å. There are also another two narrow necks at $Z\sim45$ Å and $Z\sim55$ Å, with the radius of 2.5 and 3.5 Å, respectively. At positions of the open mouth and the intracellular part, namely, the two ends of the channel, the radii are about 4 Å. In this paper, it is supposed that the interaction between particle and monomer satisfies the 12-6 LJ potential with a distance constant of 2 Å. Hence in most cases, at the three narrow necks there are attracting wells during the particle's permeation. For the outer sides of the subunits, it is observed that the radii do not change very much except at the place near to the open mouth. In general, the radius of the outer sides is around 6 Å. At the open mouth the radius increases to about 7 Å. This is because there are two loops in this region. From Fig. 1(c), it can be obviously seen that the interior structure of the channel is complex, and will affect the particle's permeation.

Clearly, the model channel has many resemblances to the natural proteins, such as the cross angles, the length, and the inner radius. These coincidences make the model take the "real" biological ion channel as prototype.

B. Single particle permeation

In Fig. 2, two individual trajectories of typical permeation processes are presented. The friction coefficients in Figs. 2(a) and 2(b) are $\xi=0.05$ and $\xi=1.0$, respectively. The driving force in both cases is $F_d=0.2$. The initial position of the particle is 10 Å above the open mouth of the model channel. In Fig. 2(a), the particle enters the open mouth ($Z\sim55$ Å) at 5×10^5 time steps. After a very short time of staying at the open mouth, the particle jumps to $Z\sim45$ Å and vibrates around this place for about 2×10^5 time steps. Then starting from 7.5×10^5 time steps, the particle goes down abruptly to $Z\sim30$ Å and oscillates around this position for about 1.7×10^6 time steps before permeating out of the channel. Whereas in Fig. 2(b), the particle enters the open mouth at about 2×10^6 time steps. Beginning at 2.2×10^6 time steps, the particle declines quickly to $Z\sim45$ Å and moves around for about 0.7×10^6 time steps. Then starting from 3×10^6 time steps, the particle walks down suddenly to $Z\sim30$ Å. After vibrating at this place for about 6.4×10^6 time steps, the particle moves out of the channel. In these two cases, the total permeation time is around 4 and 15 ns, respectively, which are in qualitative accordance with the experimental observations and the full-atom simulation results.[18]

It can be seen from Figs. 2(a) and 2(b) that the selection rates τ_S (the time steps needed to enter the open mouth) are 5×10^5 and 2×10^6 time steps, respectively. The permeation times τ_M are 2×10^6 and 7.4×10^6 time steps, accordingly. Hence, compared with the total permeation time, the selection rate is indeed very fast. Thus the neglect of selection rate in studying the permeation will not bring about large errors at least in this model.

Another common phenomenon in both cases of Fig. 2 is the long time vibration of the particle at positions around $Z\sim45$ Å and $Z\sim30$ Å. And it is obvious that in both cases, the time staying at $Z\sim30$ Å is much longer than that at $Z\sim45$ Å. This is the result of what is shown in Fig. 1(c). At these two positions, the pore is narrower than that at other places. Thus the attraction from monomers traps the particle. Besides, at $Z\sim30$ Å, the radius of the pore has the overall minimal, hence the trapping time is the longest. This indicates that the permeation is hindered at these positions due to the interior structure of the channel. A comparative study of particle's passing through a structureless smooth pore shows that the particle permeates faster under the same driving force, and there are no obvious trapping positions. As a result, taking into consideration the interior structure of the channel shall be necessary in studying the permeation process.

The third common feature for the two cases of Fig. 2 is the jump from $Z\sim45$ Å to $Z\sim30$ Å, from $Z\sim30$ Å to $Z\sim20$ Å, and from $Z\sim20$ Å to $Z<0$ Å. The jumps of the first and the last one seem to be unidirectional. It is already analyzed in Fig. 1(c) that there are two narrow necks in the channel at $Z\sim45$ Å and $Z\sim30$ Å. Hence, the monomers around the necks attract the particle and prevent the particle from passing through the necks. Under the circumstance of without the driving force, it is found that the particle can jump back from $Z\sim30$ Å to $Z\sim45$ Å. Due to the existence of the unidirectional driving force, the reversal jumps can hardly happen. Anyway, the reversal jump from $Z\sim20$ Å to $Z\sim30$ Å is observed for many times during the simulations. This indicates a low energy barrier from $Z\sim20$ Å to $Z\sim30$ Å, as well as a strong attraction from $Z\sim30$ Å. The long time staying at $Z\sim20$ Å is the effect introduced by the intracellular loop. The particle is strongly attracted by the

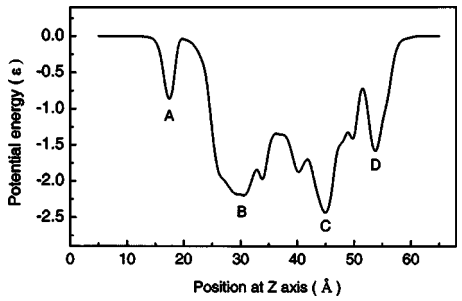

FIG. 3. The single-particle energy profile of the channel. The abscissa is the position at Z axis; the ordinate is the potential energy in reduced unit. "A," "B," "C," and "D" indicate four potential wells. The wells correspond to the narrow necks and loops of the channel.

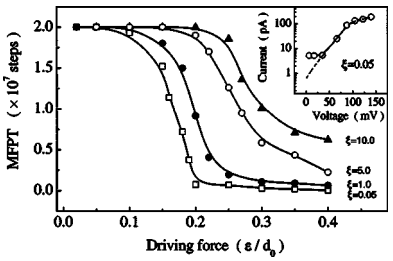

FIG. 4. The MFPT (τ_M) as a function of driving force. The simulation temperature is $T=0.1$. From up to down, the friction coefficients are 10.0, 5.0, 1.0, and 0.05, accordingly. The driving force is cut off at $F_d=0.4$. The inset is the deduced electrical current as a function of membrane voltage. The dashed line in the inset is extrapolated from the high voltage side.

monomers in and near the intracellular loop. When the intracellular loop is cut off from the model channel, it is observed that the trapping at $Z\sim 20$ Å decreases greatly. The interesting observations of relative long time staying at $Z\sim 20$ Å, the reversal jump to $Z\sim 30$ Å, and the forward jump to $Z<0$ Å imply that there shall be "permeation routes" through the channel.

For explaining more clearly the above phenomena, the single-particle energy profile is presented in Fig. 3. The energy profile is calculated by moving the particle along the bundle axis (see Sec. II). It can be seen that there are three major potential minima in the channel sited at $Z\sim 30$ Å, $Z\sim 45$ Å, and $Z\sim 54$ Å. Besides, at $Z\sim 18$ Å, there is also a shallow potential well. The four potential wells are denoted by "A," "B," "C," and "D" from the left to the right, respectively. The energy barriers from right to left are $\Delta U_{D\to C}\sim 0.8$, $\Delta U_{C\to B}\sim 1.1$, $\Delta U_{B\to A}\sim 2.2$, and $\Delta U_{A\to I}\sim 0.9$, accordingly. In which, $A\to I$ is the process from well A to the intracellular. The energy barriers in the reversal direction are $\Delta U_{A\to B}\sim 0.9$, $\Delta U_{B\to C}\sim 0.9$, $\Delta U_{C\to D}\sim 1.7$, and $\Delta U_{D\to E}\sim 1.6$, respectively. Where the process of $D\to E$ is from well D to the extracellular. Hence, in the case of no driving force, due to the diffusion movement, particle may have the probability to drift from the right to the left, which corresponds to the direction from the extracellular to the intracellular; or drift in the reversal direction as well. However, while adding the driving force on the particle, the direction from extracellular to intracellular is preferred. All the energy minima in the graph are in accordance with the structural profile in Fig. 1(c) and the trajectories in Figs. 2(a) and 2(b). It can be seen that the highest energy barrier is that from $Z\sim 30$ Å to $Z\sim 20$ Å. Thus, particle shall be trapped at $Z\sim 30$ Å for the longest time. And because the potential well at $Z\sim 18$ Å is very shallow, under the random movement, it is possible for the particle to jump back into the channel.

Figure 4 is the MFPT (τ_M) as a function of driving force under different friction coefficients. The maximal driving force is cut off at $F_d=0.4$, since this value is already much higher than that of the natural situation. From up to down, the friction coefficients are 10.0, 5.0, 1.0, and 0.05, accordingly. It shall be addressed that the horizontal lines at the top of the figure are definitely caused by the cutoff effect due to the limitation on the total simulation time. Long time behavior is not included in this paper. It is clear from the graph that there is a threshold value of the driving force for each curve, below the threshold value, the MFPT is near to or longer than 2×10^7 time steps. According to the simulation assumptions, these permeations cannot be observed. The threshold value of the driving force can be defined as where the MFPT is 90% of the maximal simulation steps, i.e., 1.8×10^7 time steps. It can be seen that the threshold value increases with the friction coefficient. Under four friction coefficients, the threshold values are $F_d=0.12$, 0.15, 0.2, and 0.25, accordingly, which correspond to membrane voltages of 36, 45, 60, and 75 mV, respectively.

In the case of $\xi=0.05$, the curve shows that when the driving force is less than 0.1, $\tau_M\sim 2\times 10^7$. These permeations are actually not observable. When the driving force is enhanced to 0.2, the permeation becomes very fast with $\tau_M\sim 10^6$ time steps. The variation rate of MFPT with driving force is $Q_F=\Delta\tau_M/\Delta F$. In the force range of 0.12–0.2, $Q_F\sim -2.1\times 10^8$. The negative sign shows that with increase in the driving force, the MFPT decreases. The sharp slope indicates that a small change in the driving force leads to a huge variation of MFPT. That is the transition from block state to permeable state. It happens within a very small range of driving force. Hence, the particle is either passing or not passing through the channel. The above range of driving force could be regarded as a transition range. By taking into consideration that $F_d\sim 0.2$ is comparable to a membrane voltage of 60 mV and MFPT $\sim 10^6$ means a real time of about 3 ns. It can be ascertained that the process of $\xi=0.05$ in Fig. 4 is similar to a voltage-gating permeation process. It is interesting to point out that when $F_d=0.2$ and $\xi=1.0$, the real permeation time is around 15 ns which is more similar to the natural situation. With the increase of friction coefficient, resemblant trends are also observed.

More interestingly, with the increase of ξ, the driving force (i.e., the relative membrane voltage) needed for proceeding the gating will increase too. For $\xi=1.0$, 5.0, and 10.0, the required driving force are 0.25, 0.35, and 0.4, respectively. The slope of Q_F at the transition range is flatter at higher friction coefficients than at lower friction coefficients. For $\xi=1.0$, 5.0, and 10.0, the gating occurs at $0.14\leqslant F_d\leqslant 0.24$, $0.21\leqslant F_d\leqslant 0.3$, and $0.25\leqslant F_d\leqslant 0.35$, accordingly. The slopes of Q_F are -1.6×10^8, and -1.2×10^8, and -1.0×10^8, respectively. Anyhow, these are still the threshold values for the driving force. It can also be seen that the minimal permeation time increases as ξ increases. For $\xi=0.05$ and

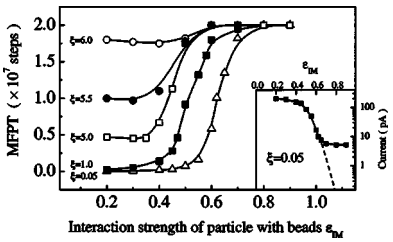

FIG. 5. The change of MFPT along with the interaction strength between monomer and particle. The temperature is $T=0.1$ and the driving force is $F_d=0.2$. From up to down, the friction coefficients are 6.0, 5.5, 5.0, 1.0, and 0.05, respectively. The inset is the relation between electrical current and ε_{IM}. The dashed line is extrapolated from the low limit of ε_{IM}.

1.0, the final minimal MFPT is around 10^6 time steps. The values of final MFPT increase to 2.3×10^6 and 6.3×10^6 at $\xi=5.0$ and 10.0, respectively. In the case of $\xi=5.0$, when $F_d\geqslant0.3$, Q_F changes from -1.2×10^8 to -3.6×10^7 time steps. Thus, with the increase in driving force, the MFPT continues to decrease. When $\xi=10.0$, a similar trend is also observed. Given the driving force $F_d\geqslant0.33$, Q_F becomes -2.4×10^7. So, the trend of Q_F at high friction coefficients of $\xi\geqslant5.0$ is slightly different from what happens at low friction coefficients. Although with further increase in the driving force, the MFPT will decrease continuously. The transition of Q_F becomes flat. This indicates that at high limit of friction coefficients, mechanisms other than pure gating dominate the process.

The inset in Fig. 4 is the deduced electrical current as a function of membrane voltage. The particle is assumed to be monovalence. The graph is taken at $\xi=0.05$. The dashed line is the extrapolated data because the finite simulation steps reduce the accuracy of electrical current at the low limit of voltage. The current increases almost exponentially with voltage in the moderate range of voltage. Then at high voltage limit, there seems to be a saturated value of about 200 pA. When the friction coefficient is increased to $\xi=5.0$, the saturated current is around 10 pA (data not shown). Hence, the selection rate also has important influence on the current. These results are in qualitative accordance with that obtained by other simulation protocols.[22,23,34]

Figure 5 is the influence on MFPT of interaction strength between monomer and particle. From up to down, the friction coefficients are $\xi=6.0$, 5.5, 5.0, 1.0, and 0.05, respectively. In general, when the interaction strength between monomer and particle is strong enough, the permeation is fully terminated. The trajectory analysis shows that the particle is trapped in the channel or diffused out of the channel. The uplimit of interaction strength at which the permeation is stopped, is also set at where the MFPT is 90% of the maximal simulation steps. For $\xi=0.05$, 1.0, 5.0, 5.5, and 6.0, the relevant uplimits of interaction strength are 0.7, 0.6, 0.53, 0.52, and 0.48, respectively. Hence, the smaller the friction coefficient, the easier the particle can pass through the channel. Decreasing the interaction strength continuously, the MFPT will decrease and incline to a stable value. For $\xi=0.05$, 1.0, 5.0, 5.5, and 6.0, the stable values of MFPT are 10^4, 10^5, 5×10^6, 1×10^7, and 1.8×10^7 time steps, accordingly. At high friction coefficients of $\xi>6.0$, due to the limitation on the maximal simulation steps, the changes in MFPT cannot be observed. According to the previous assumptions, the permeation is stopped. It is interesting to compare Q_ε under various friction coefficients, where $Q_\varepsilon=\Delta\tau_M/\Delta\varepsilon_{IM}$ is the variation rate of MFPT as a function of interaction strength ε_{IM}. The data in the transition ranges are 1.2×10^7, 5×10^7, 8×10^7, 1×10^8, and 3.1×10^8 time steps from up to down, accordingly. High friction coefficient has flat transition rate whereas low friction coefficient has sharp slope.

The graphs in Fig. 5 provide a picture of selection mechanism. Particles having strong interaction with monomers cannot pass through this channel. Hence, this channel selects particles which have weak interaction with monomers taking into consideration that the interaction between particle and monomer is LJ potential. Having a large Vdw radius leads to the same effect of strong attraction as having strong interaction strength does. In this way, this channel will also select particles which have small Vdw radius. Further simulations show that the uplimit of the Vdw radius is about 2.5 Å. It can also be expected that, especially in the artificially synthesized channels, when the water molecules in the channel are replaced by other kinds of molecules, the interaction strength between particle and monomer shall be very much different from the previous one. As a result, the permeation process will be affected greatly.

The inset of Fig. 5 is the variation of current with the interaction strength ε_{IM}. This chart is calculated with $n_q=1$ and $\xi=0.05$. The dashed line is also the extrapolated data. Clearly, at low interaction limit, the electrical current is saturated to about 200 pA. This indicates that the interior structure of the channel has nearly no influence on the permeation process. While at strong interaction limit, the dashed line shows that the current reduces to zero almost exponentially.

Figures 6(a) and 6(b) show the temperature effect on the particle's permeation. It is important to acquire the knowledge of temperature influence on biological bodies since many creatures have a favorable living temperature. In Fig. 6(a), the temperature is cut down at $T=0.3$, because at higher temperatures, the conformational distance δ (Ref. 35) shows that the conformation of the model channel distorts a lot and makes the channel no longer physically interesting. It can be seen in this figure that when the temperature is too low, the particle is "frozen," and no permeation is observed. With increase in the temperature, the particle starts to pass through the channel. The gating temperature where the permeation begins, is also defined as where the MFPT is 1.8×10^7 time steps. So the gating temperatures are 0.04, 0.06, 0.08, 0.082, and 0.084 for $\xi=0.05$, 1.0, 2.0, 3.5, and 4.0, respectively. The relevant Q_T is defined as $Q_T=\Delta\tau_M/\Delta T$, the data in the fastest descending areas (the transition range) are -2.1×10^8, -2.3×10^8, -3.3×10^8, -1.5×10^8, and -1×10^8, accordingly. Thus, in the middle range of friction coefficient, i.e., $1.0\leqslant\xi\leqslant2.0$, the changes of Q_T are bigger than that in other ranges. This could be regarded as the "temperature induced gating," i.e., in the specific range of temperature, the small change in the temperature may bring about huge influence on the permeation.

Further increasing the temperature, particles at low friction coefficient will have a stable value of MFPT. They are

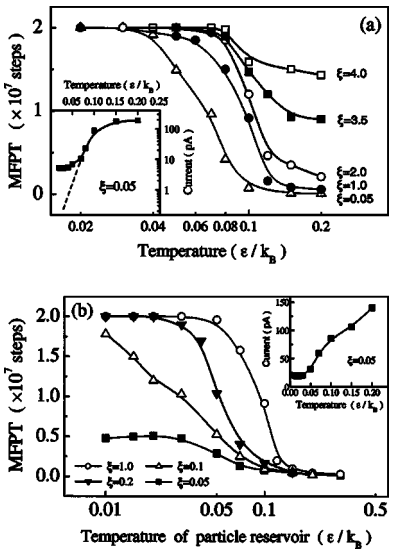

FIG. 6. The influence of temperature on the MFPT. The abscissa is the temperature in a log base and the ordinate is the MFPT. The driving force is $F_d=0.2$. (a) Both the particle reservoir and monomers have the same temperature, and the uplimit of temperature is set at $T=0.3$. The friction coefficients from left to right are $\xi=4.0$, 3.5, 2.0, 1.0, and 0.05, respectively. (b) Only the temperature of particle reservoir is changeable. The temperature of monomers is set to be 0.1. From up to down, the friction coefficients are $\xi=1.0$, 0.2, 0.1, and 0.05, accordingly. The insets are the currents as functions of channel temperature and the temperature of particle reservoir. The dashed line is extrapolated from the high limit of temperature.

$\tau_M \sim 5\times10^4$, 2×10^5, and 3×10^6 time steps for $\xi=0.05$, 1.0, and 2.0, respectively. When the friction coefficients are raised to $\xi=3.5$ and $\xi=4.0$, the final stable values in the simulations are around 0.9×10^7 and 1.5×10^7 time steps, accordingly.

The inset in Fig. 6(a) shows that the current increases exponentially with the temperature. The calculation parameters are the same as before. The relation between current and temperature is qualitatively similar to the experimental findings.[36]

In Fig. 6(b), we can see another man-made situation where the temperature of particle reservoir is supposed to be different from the temperature of channel. It could come true when putting a hot channel (cell) into cold particle reservoir, or on the contrary, putting a cold channel into hot particle reservoir. The friction coefficients used here are $\xi=1.0$, 0.2, 0.1, and 0.05 from up to down, accordingly. The curves in this figure are quite different from what in Fig. 6(a). At the limit of high temperature of particle reservoir, particle runs through the channel very quickly. It seems to be an identical MFPT of $\tau_M \sim 10^5$ time steps at various friction coefficients. Anyway, at the side of low temperature of particle reservoir, different friction coefficients have different pictures. When $\xi=0.05$, the low-temperature particle has a saturated MFPT which is about 5×10^6 time steps. And $Q_T \sim -7\times10^7$ time steps at the transition range. At the situation of high friction coefficient, i.e., $\xi=0.2$ and 1.0, the MFPTs reach the maximum value (2×10^7) relatively fast. The values of Q_T are -2.9×10^8 and -2.2×10^8, accordingly. For the middle case of $\xi=0.1$, the value of Q_T is about -1.8×10^8. It is clear that the MFPT increases almost exponentially when decreasing the temperature of particle.

It is interesting to compare the different behaviors at low friction coefficient (i.e., $\xi=0.05$) between Figs. 6(a) and 6(b). The difference is when both the temperatures of particle reservoir and of channel are low, the permeation can hardly occur. But when only the temperature of particle reservoir is low, the particle can pass through the channel within a very limited time steps. For example, in Fig. 6(a), when $T=0.03$, $\tau_M \sim 2\times10^7$ which indicates the permeation is actually not observable in the simulations. But in Fig. 6(b), at the same temperature, $\tau_M \sim 5\times10^6$. This is a rather quick permeation process. The analysis on typical trajectories shows that when the temperatures of particle reservoir and of channel are low, the particle is trapped at the two narrow necks of the channel ($Z\sim45$ Å and $Z\sim30$ Å) for much longer time steps. The conformational analysis denotes that in this circumstance, the radii of the channel at $Z\sim45$ Å and $Z\sim30$ Å are 2.74 and 2.44 Å, respectively. When only the temperature of particle reservoir is low, the average radii at these two positions are 2.86 and 2.83 Å, accordingly. The former ones are apparently smaller than the latter ones. That is to say, when the channel is cool, it shrinks and makes the necks of the channel narrower than that at higher temperatures. It shall be complemented that the radii of channel discussed here are calculated when the particle is embraced in the channel. In the case of without particle in the channel, the radii are smaller than that with particle in it.

The inset in Fig. 6(b) is the relation of current with the temperature of particle reservoir. All parameters are the same as mentioned above. It is interesting to note that the *I-T* relation can be divided into two sections and both seem to be linear. At low temperature of particle reservoir, the current is saturated at around 20 pA, while at high temperature of particle reservoir, the current increases almost linearly with the temperature of the particle reservoir.

C. Multiparticle permeation

It is more realistic to consider the situation involving many particles in the whole permeation process. The simplest one is that there are many particles at the extracellular side, and each time only one particle is allowed to run through the channel. Only after this particle reaches the intracellular side, the second particle is permitted to enter the channel. In all the simulations, when two or three particles are put at the extracellular side, the permeation is observed to be almost the same as the one-particle situation. Because in this model, the repulsive interaction distance between particles is one order less than the thickness of membrane or the dimension of the particle reservoir. Hence, when only one particle is allowed to enter the channel, the increase in particle number in the extracellular part is equal to weakly enhancing the repulsion between particles in the particle reservoir. As a result, the selection rate only has slight changes. Meanwhile, MFPT is dominated by the internal structure of the channel and will not be affected much by the repulsion. Consequently, the permeation behaviors are similar to the one-particle situation.

Anyhow, the more important situation involves many

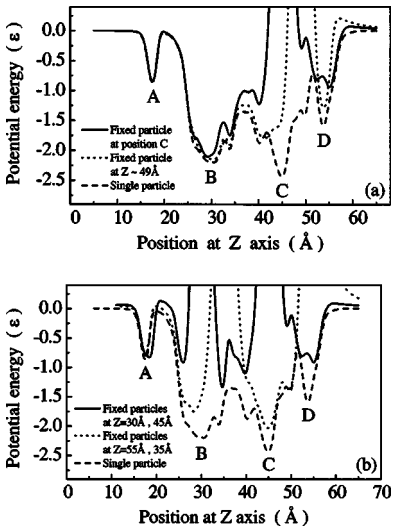

FIG. 7. The multiparticle energy profiles. The dashed line is the single-particle energy profile, which is the same as in Fig. 3. A, B, C, and D are relevant four energy wells. (a) The two-particle energy profile. The solid line is the energy profile for the second particle when the first particle is fixed at $Z=45$ Å, in the channel. The dotted line is energy profile of the first particle when the second particle falls into the energy well at $Z\sim 49$ Å. (b) The three-particle energy profile. The solid line is the energy profile of moving the third particle along Z axis when the first two particles are set at $Z=30$ Å, and $Z=45$ Å. The dotted line is the energy profile of the first particle when the second and the third particles are placed at $Z=35$ Å and $Z=55$ Å, respectively.

particles in the channel simultaneously. Figure 7 is the energy profiles when particles are set at specific positions of the channel.

The two-particle situation is shown in Fig. 7(a). The dashed line is the single-particle energy profile (see Fig. 3). The solid line shows the influence of the first particle, which is set in the channel in advance, on the second particle which enters the channel later than the first particle. The first particle is chosen to site in the channel at $Z=45$ Å. Because as shown by the dashed line, the potential energy is the overall minimum at this point. For any particle entering the channel in advance, this position shall be the most favored one. It can be seen from Fig. 7(a) that compared with the single-particle energy profile, the two-particle energy profile changes greatly at places where $35<Z<56$ Å. The deepest potential well at $Z\sim 45$ Å in the single-particle circumstance becomes a huge energy barrier. The potential well at position D splits into two wells sited closely at $Z\sim 52$ Å and $Z\sim 55$ Å with the depth of -0.8 and -0.9, respectively. Besides, there is additionally a small potential well at $Z\sim 49$ Å. These energy minima play important roles in the dynamic energy profile. The potential well at $Z\sim 40$ Å is also lifted up, with the barrier to position B decreased from 0.5 to 0.2. As a result, in almost one half of the channel, all the potential wells become shallow. Thus, the later-coming particles are not easy to trap in these wells.

The dotted line gives the change of energy profile when the second particle enters the channel and resides at $Z\sim 49$ Å. This is a "dynamic energy profile" since a part of the dynamic behaviors are taken into consideration in drawing this energy profile. From the solid line, it is apparent that the second particle can jump to $Z\sim 49$ Å where there is a small energy well. At this time, the distance between the first and the second particle is short enough to have strong repulsion. Hence, the energy profile of the first particle will also be changed as shown by the dotted line. It is clear that compared with the single-particle energy profile, the previously deepest potential well at $Z\sim 45$ Å becomes an energy slope. The position of the potential well is translated to $Z\sim 42$ Å. The barrier to position B becomes shallow from 1.1 to 0.5. That is to say that when the second particle stays in the well at $Z\sim 49$ Å, the first particle will be propelled to the new well at $Z\sim 42$ Å. In addition, since the barrier to position C is decreased greatly, the first particle can overcome this barrier and permeate more easily to the well at $Z\sim 30$ Å.

The three-particle situation is presented in Fig. 7(b). The dashed line is also the single-particle energy profile. The solid line is the energy profile when the first two particles are placed at $Z=30$ Å and $Z=45$ Å, respectively. It can be seen that all the potential wells in the channel are lifted up. The previous three wells at $Z\sim 30$, 45, and 54 Å are transformed into five wells located at $Z\sim 26$, 35, 40, 52, and 55 Å, respectively. The previous well depths are -2.2, -2.4, and -1.6; the new well depths are -0.9, -1.3, -1.1, -0.8, and -0.9, accordingly. There is still a small potential well at $Z\sim 49$ Å with the depth of about -0.3. It can also be expected that the permeation process may be speeded up because the wells are shallower than before.

The dotted line is the dynamic energy profile for three-particle process. The first two particles are located in advance in the channel at the same places as mentioned above. Previously in Fig. 7(a) it has been shown that, when there is a particle at $Z=45$ Å, the potential wells at around $Z\sim 55$ Å become shallow and a small new potential well is created at $Z\sim 49$ Å. When the third particle enters the channel and jumps into this small new well, the second particle located at $Z=45$ Å will be pushed to the well at $Z\sim 40$ Å. Then, as shown by the solid line of Fig. 7(b), due to the existence of the first particle which is in the channel at $Z\sim 30$ Å, there shall be another small energy well at $Z\sim 35$ Å. Since the barrier from $Z=40$ Å to $Z=35$ Å is only 0.55, the second particle can overcome this barrier and jump to $Z\sim 35$ Å. Then the first particle previously sited at $Z=30$ Å will be strongly excluded. It is obvious from the dotted line that the well previously at $Z\sim 30$ Å moves to $Z\sim 28$ Å, and the barrier to position A is changed from 2.2 to 1.8. In the meantime, because the particle previously at $Z\sim 45$ Å moves to $Z\sim 35$ Å, it can be seen that the barrier at $Z\sim 45$ Å becomes a potential well. Hence, the particle in the small well at $Z\sim 49$ Å becomes energetically beneficial to the position of $Z\sim 45$ Å. In this way, the permeation process may be accelerated. The experiments and other simulations on potassium channels also support a three-ion permeation mechanism.[37]

In order to show the detailed permeation process when three particles are in the channel simultaneously, we present the trajectories of three particles in Fig. 8. Originally, two particles reside at $Z\sim 30$ Å and $Z\sim 45$ Å, respectively. When the third particle enters the channel to $Z\sim 55$ Å, the first particle at $Z\sim 30$ Å moves out of the channel very quickly and the trajectory is not shown in the graph. Then,

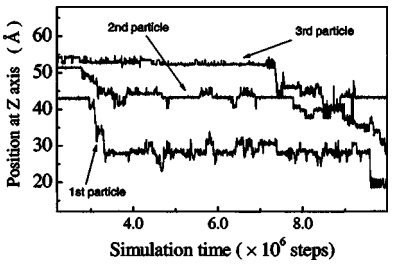

FIG. 8. The typical permeation process involving three particles. The simulation is performed under temperature of $T=0.1$ and driving force of $F_d=0.2$. Two particles reside at $Z\sim 45$ Å and $Z\sim 55$ Å in advance, then the third particle enters the channel. The lowest line is the trajectory of the first particle, the middle line is for the second, and the up line is for the third particle.

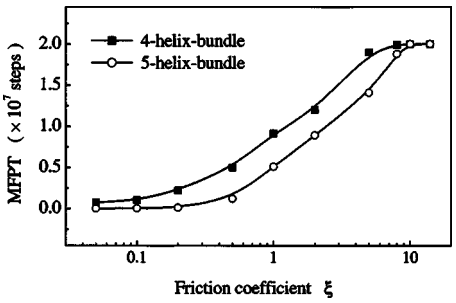

FIG. 9. The comparison of permeation time between five-helix-bundle and four-helix-bundle under different friction coefficients. The simulation is at temperature of $T=0.1$ and under driving force of $F_d=0.2$. The filled square is for the four-helix-bundle; the blank circle is for five-helix-bundle. The abscissa is the friction coefficient in a log base, and the ordinate is the MFPT.

there are now only two particles in the channel residing at $Z\sim 45$ Å and $Z\sim 55$ Å, accordingly. These two particles are denoted by the first and the second particle, respectively. After that, a new third particle enters the channel very quickly. Thus, there are again three particles in the channel, the whole permeation process is still a three-particle process. It is apparent that when the third particle runs into the channel, it will find the potential wells at around $Z\sim 55$ Å. The second particle is first propelled forward slightly. Then starting from 2.8×10^6 time steps, the second particle takes a big jump to $Z\sim 45$ Å while the third one stays in the well at $Z\sim 52$ Å. Under the influence of second particle, starting from the 3×10^6 time steps, the first particle is pushed to $Z\sim 40$ Å and $Z\sim 35$ Å for interim. Then beginning from 3.3×10^6 time steps, the first particle jumps to the well at $Z\sim 28$ Å. It shall be noted that since there is a rather big chamber in the channel, hence the coordinates of different particles on Z axis may overlap, but their actual spatial distance may be long enough to avoid the strong repulsion. After a long time equilibration, starting from 7.3×10^6 time steps, the third particle tries to penetrate down the Z axis. It occupies the wells around $Z\sim 45$ Å at 7.6×10^6 time steps. The second particle is firstly repelled to $Z\sim 40$ Å at 7.8×10^6 time steps and then to $Z\sim 35$ Å at 9.2×10^6 time steps. Under this influence, beginning at 9.6×10^6 steps, the first particle is pushed to $Z\sim 20$ Å. At this time, the second and the third particles reside at positions of $Z\sim 28$ Å and $Z\sim 45$ Å, respectively. When the first particle is expelled out of the channel, another particle shall enter the open mouth from the extracellular, and a new permeation circulation begins.

D. Permeation through a five-helix-bundle

It is interesting to generalize the above approach to a five-helix-bundle ion channel, such as the common ion channel of MscL,[7] and compare the result of permeation with that of four-helix-bundle. In the native state of the ion channel MscL, five independent helices are assembled together to form a bundle. Thus a cavity is encompassed in the interior of the bundle. It is obvious that the construction and alignment of helices are very similar to that of the four-helix-bundle channel KcsA studied above. The construction of five-helix-bundle from arbitrary initial conformation is somewhat difficult and hence needs further study. However, since what we are interested in now is only the permeation process, it is reasonable to choose a five-helix-bundle as the initial conformation and adopt potential parameters which can keep the stability of this conformation. For this purpose, a set of potential parameters is chosen as follows, i.e., $A_\phi=B_\phi=C_\phi=2.3$ and $D_\phi=0.1$ for the dihedral angle potentials, $\lambda=2.1$ and $\sigma_{ij}=1.4d_0$ for the Lennard-Jones interactions. The mass of each monomer is increased to $m_{\mathrm{New}}=100$ m to mimic the complex structure of the real pentameric ion channel. All other parameters and the interaction between particle and monomers are kept unchanged. In such a way, the five-helix-bundle during the simulation will vibrate around its equilibrium position where there is a cavity in the interior. Hence, the particle may pass through the five-helix-bundle under the undirectional force.

Figure 9 shows the results of permeation of the particle through a five-helix-bundle under different friction coefficients compared with that through a four-helix-bundle. It is a clear that the permeation properties of these two circumstances are very similar. At the low limits of the friction coefficient, the permeation is very fast and the particle runs through the bundle within 10^5 time steps, while at the higher friction coefficients, the permeation is slowed down and finally reaches the saturated value of 2×10^7 time steps. However, the permeation time of the particle through the five-helix-bundle is always much faster than that through the four-helix-bundle. For example, when $\xi=1.0$, the MFPT for five-helix-bundle is 5.1×10^6 time steps, while MFPT for four-helix-bundle is 9.2×10^6 time steps. Such variation of the permeation time mainly originates from the difference of internal structures between two kinds of bundles. Conformation analysis shows that the minimum diameter of the internal cavity for the four-helix-bundle channel is about 4 Å, while in the five-helix-bundle, the minimum diameter for the internal pore is around 10 Å. However, the relative positions of different helices of the five-helix-bundle deviate obviously from the real situation. This is the limitation of our present approach. Hence the generalization of five-helix-bundle needs further study.

IV. SUMMARY

A coarse-grained model of four-helix-bundle protein is applied to mimic the ion channel. The analysis on the struc-

tural properties shows that the cross angles between subunits of the four-helix-bundle and the distribution of monomers are very similar to that of the natural ion channels. The diameter of the internal cavity of the model channel is also very resemblant to that of ion channels observed in experiments.

It is found that the permeation process depends greatly on the interior structure of the model ion channel. The study on both the conformation and energy profile shows that the narrow necks in the channel trap the particle and prevent it from passing through the channel.

This model shows the characteristic of gating induced by driving force, which is comparable to the static membrane voltage on the cell. The smaller the drying force, the slower the permeation is. The temperature also has strong influence on the permeation process. Generally, raising the temperature will speed up the permeation. Besides, the strong interaction strength between the monomer and the particle obstructs the permeation. For particles having the same interaction strength, the larger the Vdw radius, the slower is the particle permeation. In addition, there is an uplimit of the Vdw radius for the permeable particles. In one word, the channel has the selectivity on particles of small radius or of weak interaction with monomer. It shall be noted that this is not the real selectivity mechanism. As we know, almost all ion channels are composed of complicated combination of many different domains. All these domains may contribute to the stability of the structure or the functions of the ion channel. Furthermore, specific amino acid may also greatly influence the functions of the ion channel. Hence, a coarse-grained model is indeed too simple to explain the selectivity mechanism, especially when this model does not retain all the domains of the real ion channel, although this model provides interesting information of the particle on the permeation process. It seems clear that in order to explain the selectivity mechanism, the full-atom model or other advanced models are needed.

The friction coefficient in the channel also plays an important role in the permeation process. It is observed that with the increase of the friction coefficient, the simulation steps needed by the particle to pass through the channel increases. The smaller friction coefficients used in this paper have been widely applied in coarse-grained protein folding simulations and are in accordance with Kramer's low limits.[30,35] It has been argued by Cieplak and co-workers,[35] as well as Onuchic and collaborators,[38] that the viscous friction may have almost linear impact on the system. It is expected that the smaller fictions can still give an approximate illustration on the physical picture of the permeation. It seems that the use of a small friction (viscosity) is based on the model itself. Since some interaction terms, such as the explicit interaction of the amino acids with the water molecule, are implicated in the effective Lennard-Jones term. Therefore, the friction for the particles is an effective one. It is expected that due to the small number of water molecules in the nanoscale space within the interior of the ion channel, the postulation of continuum fluid is no longer eligible. The friction of water molecules shall be explained by the collisions between water molecules and the passing particle. Hence, the friction coefficient deduced from the continuum fluid may be different from the effective friction coefficient which is obtained by the collisions between water molecules and particle. Under the elastic collision mechanism, the velocity of the particle after the collision is about 6% of the velocity before the collision. On the other hand, when the effective friction coefficient of 0.05 is used, the velocity decreases to 7% of the initial velocity after a time period which is comparable to the interval between two consecutive collisions. These results indicate that the effective friction coefficient used in this paper is a reasonable approximation to mimic the collision mechanism. In order to check the influence of friction on the permeation, we have simulated the permeation of particles by adopting higher frictions. The highest friction coefficient corresponds to the viscosity of N_a^+ in water at room temperature, which makes the friction coefficient at the order of 100 in reduced unit. The results show that the bigger the viscosity, the more time the particle needs to drift, and also the bigger is the driving force needed. However, the basic physical pictures and the trends are almost the same. It is interesting to note that in the artificially synthesized ion channels, the internal water molecules may be replaced by other small molecules. Hence, the internal friction coefficient should be very different from that of water molecules and have more significant influence on the permeation. It is obvious that the effective friction coefficient used in this paper is chosen relevant to the real situation for obtaining reasonable results. Although these friction coefficients are normal in coarse-grained protein folding researches, the best way of matching the experimental requirements is the application of full-atom molecular dynamics.

The generalization of this coarse-grained approach to five-helix-bundle shows that the basic permeation physics is quite similar to that for four-helix-bundle. However, the conformational properties of the five-helix-bundle deviate from the experimental observations of homopentamer ion channel. Hence, further studies to the approach and on the process are needed.

Through the analysis on the multiparticle energy profile, the dynamic energy profile and the multiparticle trajectories, it is found that the four-helix-bundle model channel prefers to take a multiparticle permeation protocol. Although this result can be easily achieved by the comparison of MFPTs between various conditions, it is interesting to use above mentioned protocols to present the detailed dynamic information on the permeation processes. With two or three particles residing in the channel simultaneously, the energy wells become shallow and hence facilitate the permeation. In an actual three-particle process, when the third particle is attracted into the channel by the monomers, the first particle which is set to be the closest to the intracellular will penetrate first under the effect of driving force together with the repulsion from the second and the third particles. Then the second particle takes the position previously occupied by the first particle, and the third particle goes to the place where the second particle was. This is one circle of the three-particle permeation process.

ACKNOWLEDGMENTS

This work was supported by the National Natural Science Foundation of China (Grant Nos. 90103031, 10474041, 90403120, and 10021001), and the Nonlinear Project 973 of NSM (Grant No. G2000077300).

[1]D. A. Doyle, J. M. Cabral, R. A. Pfuetzer, A. Kuo, J. M. Gulbis, S. L. Cohen, B. T. Chait, and R. Mackinnon, Science **280**, 69 (1998).
[2]C. Branden and J. Tooze, *Introduction to Protein Structure* (Garland, New York, 1998).
[3]Y. X. Jiang, A. Lee, J. Y. Chen, M. Cadene, B. T. Chait, and R. Mackinnon, Nature (London) **417**, 523 (2002).
[4]L. H. Pinto, G. R. Diechmann, C. S. Gandhi *et al.*, Proc. Natl. Acad. Sci. U.S.A. **94**, 11301 (1997).
[5]S. Geib, G. Sandoz, K. Mabrouk *et al.*, Biochem. J. **364**, 285 (2002).
[6]G. Chang, R. H. Spencer, A. T. Lee, M. T. Barclay, and D. C. Rees, Science **282**, 2220 (1998).
[7]C. Adcock, G. R. Smith, and M. S. P. Sansom, Biophys. J. **75**, 1211 (1998).
[8]P. S. Phale, T. Schirmer, A. Prilipov, K. L. Lou, A. Hardmeyer, and J. P. Rosenbusch, Proc. Natl. Acad. Sci. U.S.A. **94**, 6741 (1997).
[9]T. Schirmer and P. S. Phale, J. Mol. Biol. **294**, 1159 (1999).
[10]L. Song, M. R. Hobaugh, C. Shustak, S. Cheley, H. Bayley, and J. E. Gouaux, Science **274**, 1859 (1996).
[11]P. J. Cragg, Sci. Prog. **85**, 219 (2002).
[12]Y. Kobuke, K. Ueda, and M. Sokabe, J. Am. Chem. Soc. **114**, 7618 (1992).
[13]R. G. Ghadiri, J. R. Granja, R. A. Milligan, D. E. McRee, and N. Khazanovich, Nature (London) **366**, 324 (1993).
[14]O. Murillo, S. Watanabe, A. Nakano, and G. W. Gokel, J. Am. Chem. Soc. **117**, 7665 (1995).
[15]N. Unwin, Nature (London) **373**, 37 (1995).
[16]S. Bernèche and B. Roux, Nature (London) **414**, 73 (2001).
[17]L. R. Forrest, A. Kukol, I. T. Arkin, D. P. Tieleman, and M. S. P. Sansom, Biophys. J. **78**, 55 (2000).
[18]I. H. Shrivastava, D. P. Tieleman, P. C. Biggin, and M. S. P. Sansom, Biophys. J. **83**, 633 (2002).
[19]Q. F. Zhong, Q. Jiang, P. B. Moore, D. M. Newns, and M. L. Klein, Biochem. J. **74**, 3 (1998).
[20]T. W. Allen, T. Bustuğ, S. Kuyucak, and S. H. Chung, Biophys. J. **84**, 2159 (2003).
[21]T. W. Allen, S. Kuyucak, and S. H. Chung, Biophys. J. **77**, 2502 (1999).
[22]S. H. Chung, T. W. Allen, M. Hoyles, and S. Kuyucak, Biophys. J. **77**, 2517 (1999).
[23]B. Corry, T. W. Allen, S. Kuyucak, and S. H. Chung, Biophys. J. **80**, 195 (2001).
[24]J. D. Lear, Z. R. Wasserman, and W. F. Degrado, Science **240**, 1177 (1988).
[25]Z. Guo and D. Thirumalai, J. Mol. Biol. **263**, 323 (1996).
[26]S. P. Ho and W. F. DeGrado, J. Am. Chem. Soc. **109**, 6751 (1987).
[27]C. Clementi, A. Maritan, and J. R. Banavar, Phys. Rev. Lett. **81**, 3287 (1998).
[28]A. Liwo, S. Oldziej, M. R. Pincus, R. J. Wawak, S. Rackovsky, and H. A. Scheraga, J. Comput. Chem. **18**, 849 (1997).
[29]M. P. Allen and D. J. Tildesley, *Computer Simulation of Liquids* (Clarendon, Oxford, 1989).
[30]T. Veitshans, D. Klimov, and D. Thirumalai, Folding Des. **2**, 1 (1996).
[31]P. F. Predki and L. Regan, Biochemistry **34**, 9834 (1995).
[32]S. Presnell and F. E. Cohen, Proc. Natl. Acad. Sci. U.S.A. **86**, 6592 (1989).
[33]A. Kohen, R. Cannio, S. Bartolucci, and J. P. Klinman, Nature (London) **399**, 496 (1999).
[34]S. Bernèche and B. Roux, Proc. Natl. Acad. Sci. U.S.A. **100**, 8644 (2003).
[35]T. X. Hoang and M. Cieplak, J. Chem. Phys. **112**, 6851 (2000).
[36]M. Kunkel, D. B. Johnstone, J. H. Thomas, and L. Salkoff, J. Neurosci. **20**, 7517 (2000).
[37]P. H. Nelson, J. Chem. Phys. **117**, 11396 (2002).
[38]H. Nymeyer, A. E. Garcia, and J. N. Onuchic, Proc. Natl. Acad. Sci. U.S.A. **95**, 5921 (1998).